2006

# Comments on the Mechanism of Aging of Antimony Doped Tin Oxide Based Electrochromic Devices

Joo C. Chan
*Portland State University*

Nicole A. Hannah
*Portland State University*

Shankar B. Rananavare
*Portland State University*, ranavas@pdx.edu

Laura Yeager
*Avery Research Center*

Liviu Dinescu
*Avery Research Center*

***See next page for additional authors***

# Comments on the Mechanism of Aging of Antimony Doped Tin Oxide Based Electrochromic Devices

Joo C. Chan, Nicole A. Hannah, Shankar B. Rananavare[†], Laura Yeager[1], Liviu Dinescu[1], Ashok Saraswat[1], Pradeep Iyer[1] and James P. Coleman[2]

*Department of Chemistry, Portland State University, Portland, Oregon 97207, U.S.A.*

[1]*Avery Research Center, Avery Dennison, Pasadena, California 91107, U.S.A.*

[2]*Albion LLC, Maryland Heights, Missouri 63043, U.S.A.*

Electrochromic effects of antimony doped tin oxide (ATO) nanoparticles are investigated to probe device yellowing (degradation). Voltage vs contrast ratio curves exhibit hysteresis, i.e., image-sticking phenomena due to irreversible charge insertion. X-ray, impedance and optical b* studies suggest that the yellowing/charge trapping is nanoparticle size-dependent with 4 nm size particles exhibiting the least yellowing. Yellowing results in increased impedances of electrode-electrolyte interface and electrode corrosion. Plausible sources of discoloration are formation of insulating complex alkali oxide film, carrier inversion (n-to-p type) through electrochemical Li doping, redeposition of the corroded electrode material and perhaps residual concentration of charge-transfer species.

**KEYWORDS:** antimony doped tin oxide (ATO), nanoparticles, electrochromism (EC), charge trapping, X-ray diffraction, electrochemical impedance, EC device degradation

[†] E-mail address: ranavas@pdx.edu

Non-stoichiometric $SnO_x$ is a rare transparent semiconductor exhibiting a large band-gap (3.6 eV) and high carrier density ($10^{19}$-$10^{21}$ $cm^{-3}$)[1]. Thin films of $SnO_x$ have been used in applications ranging from electrodes in liquid crystal display devices, solar cells to sensors[2]. Unlike the widely studied $WO_3$ based electrochromic materials[3], the intrinsic electrochromic properties of $SnO_x$ are weak but can be improved by antimony doping. Coleman *et al.* have established an optimum electrochromic performance in antimony doped tin oxide [ATO] when the mole ratio of Sb is 0.42 (= [Sb]/([Sb]+[Sn])) during sol-gel synthesis[4,5]. Nanocrystalline (casserite lattice) ATO particles (4-9 nm) are readily synthesized by this technique and upon calcination at 600°C the yellow powder transforms to a bluish color due to the presence of free electron carriers at room temperature. The conductivity exhibits a maximum at a doping level of about 5-10 atomic percent[6], which has been attributed to various mechanisms[7-9]. The Sb doping leads to n-type conductivity by creating delocalized donor atom states near the conduction band of $SnO_x$. Materials and device optimization for flexible and inexpensive displays exploiting novel *in-plane* anode-cathode configurations have been elucidated in a series of papers[4,5]. The electrochromic (EC) devices exhibit remarkable (1) memory effect (refresh times~2-24 h), (2) low-power consumption (needing only 10-100 $\mu A/cm^2$@ 1-1.2 operational voltage) and (3) reasonable contrast ratios (2-4).

The EC devices were constructed on flexible plastic substrates. Screen-printing, anodic and cathodic areas separated by plastic insulation, was achieved by successive deposition of silver paint, carbon ink (to prevent corrosion of Ag), $TiO_2$ (conductive and reflective particles) followed by an electrochromic layer of ATO nanoparticles (dispersed in Viton, a fluoroelastomer), total electro-active layer thickness $\approx$ 50 $\mu$m. The electrolyte contained 30% LiCl solution in a polymeric gel (see Fig. 1). Upon application of DC voltage, the anodic area

becomes transparent due to carrier depletion and appears white due to light reflection from the underlying $TiO_2$ layer. In the cathodic region, injection of electrons and migration of Li ions in the electrochromic layer increases its optical absorption and it appears black[7-9].

This paper examines factors affecting the device lifetime/aging, specifically the origins of distinct yellowish discoloration observed in the cathodic region during operation. Discoloration increases with the operation time and the magnitude of DC voltage. Bipolar pulse driving scheme (switching electrode polarities) reduces the extent of yellowing ($\propto$ 1/frequency). Given the mixed valence nature of both $Sn^{+4/+2}$ and $Sb^{+5/+3}$ oxides, the development of their colored charge transfer complexes was probed using Sn Mössbauer[10] and Sb X-ray absorption near edge structure (XANES) spectroscopies[11]. Sn Mössbauer spectra [Fig. 2(a)] from yellowed regions do not show presence of peak(s) at 4-6 mm/sec, characteristic of $Sn^{+2}$, neither do the antimony $L_1$ edge in XANE spectra reveal $Sb^{+3}$ ions [Fig. 2(b)]. X-ray photoelectron spectroscopy studies showed no difference in elemental composition eliminating potential source due to electrolyte/polymer degradation. Treatment with oxidizing (NaOCl) or reducing ($SnCl_2$) solutions does not alter the discoloration.

Evolution of contrast ratio (CR$\propto$injected charge), as the device is slowly (time $\approx$ 3 h) cycled between positive and negative voltages, exhibits distinct hysteresis [Fig. 3(a)] with non-zero CR at V=0, after voltage cycling. It suggests an impeded movement of ions from nanoparticulate laden electrodes, i.e., irreversibility of $Sb(V)_2O_5+4e^-+4Li^+ \leftrightarrow Li_4Sb(III)_2O_5$ reaction at cathode, similar to trapping of electrons in Si nanoparticles[12,13] embedded in transistor gates. To quantify yellowing, we measured b* (CIE 1976 color coordinate) using an Ocean Optics$^{TM}$ reflection spectrometer, 15 min after shorting anode and cathode together. For fresh and yellowed samples b* values are about 2 and >4, respectively. Figure 3(b) shows

development of b* as a function of device operation (at 1.2 V) time. b* exhibits a logarithmic growth, [b*~ $\log(t)^{0.5}$]. While experiments involving fixed charging time and variable discharge times yielded a smaller slope of –0.3. Thus, the electrochromic process appears to be only partially reversible, controlled by very slow kinetics of charge movement.

We employed impedance spectroscopy (from 5 Hz-14 MHz, HP4192 LCR meter interfaced to a PC) to study charge transport processes between the electrolyte-electrode interface. The Nyquist plots (Fig. 4) were analyzed using[14,15] Randle's equivalent circuit (Zsimp Version 3.2, from Princeton applied research); see Table I. Here $R_s$, $R_p$, and C are the high frequency solution resistance, the polarization resistance, and the net capacitance (due electrode-electrolyte double layer and a series capacitance due to depletion layer in the semiconductor) respectively; W is the Warburg impedance. $R_p$ increased (Table I) with the applied potential consistent with Volmer-Butler mechanism[14,15]. The corresponding decrease in C indicated increased depletion layer thickness[9]. The mildly yellowed samples also showed an increase in $R_p$, W, and $R_s$. For deeply yellowed samples, observed (Table I) precipitous rise in $R_p$ and W and drastic decrease in C implied electrode restructuring due to growth of an insulating barrier and electrochemical corrosion.

X-ray diffraction studies of fresh and degraded devices, Fig. 5, indicated that upon electrochromic operation, particle (grain) size decreases, especially the larger size particles. For two devices made from different nanoparticle size-distributions, we note that particles of 4 nm size undergo no further reduction in size (Table II). These devices exhibit lesser extent of yellowing (but with lower CR). This can be understood in terms of their higher columbic charging energy (~1/size) for smaller particles. Atomic absorption spectroscopy of the electrolyte from yellowed devices revealed significant amounts of Sb, Table II.

We consider yellowing mechanisms consistent with our experimental results. Although we were unable to detect charge-transfer complexes of Sn or Sb within the sensitivities of the analytical techniques employed, it is plausible that low concentrations of spatially isolated (i.e., not reversibly oxidized/reduced by chemical or electrical means) could cause yellowing. The observed decrease in the ATO-electrode particle size and the Atomic absorption detection of Sb/Sn in electrolyte implicates electrode corrosion. Migration and redeposition of electrolyte-borne corrosion products on the electrode surface could also lead to insulating colored films of complex oxides. A plausible example is cathodic formation of amorphous and sparingly-soluble $LiSb(V)O_3$[16] during grounding, through $Li_4Sb(III)_2O_5+1/2O_2 \rightarrow 4e^-+2Li^{+4}+2LiSbO_3$ reaction, involving dissolved oxygen from electrolyte or from the $SnO_x$ lattice. Also, if an electrochemical p-doping of the n-type ATO through insertion of Li ions by displacing Sb/Sn ions were to take place then resulting carrier-depleted p-n junctions could form a colored film. Reported synthesis of p-type $SnO_x$ with LiCl by high temperature pyrolytic method[17] supports this possibility. Thus, limiting the extent of Li ion insertion with uniform small-size electrochromic ATO particles (<5 nm) emerges as a new strategy for improving device-longevity.

**Acknowledgements:** We wish to thank Dr. Wolfgang A. Caliebe of Brookhaven National Laboratories for collecting Sb XANE spectra on samples.

**References**


1) Ç. Kılıç and A. Zunger: Phys. Rev. Lett. **88** (2002) 095501.
2) H. L. Hartnagel, A. L. Dewar, A. K. Jain and C. Jagadish: *Semiconducting Transparent thin Films* (IOP Publishing Ltd, Bristol, 1995) p. 358.
3) For a review see: P. M. S. Monk, R. J. Mortimer and D. R. Rosseinsky: *Electrochromism: Fundamentals and Applications* (Wiley-VCH, Weinheim, 1995) p. 3.
4) J. P.Coleman and J. H. Wagenknecht: Proc. 3rd Symposium on Electrochromic Materials, 1996, vol. **96**(24), p. 325.
5) J. P. Coleman, A. T. Lynch, P. Madhukar and J. H. Wagenknecht: Solar Energy Materials & Solar Cells **56** (1999) 395; **56** (1999) 375.
6) J. C. Volta, P. Bussiere, G. Coudurier, J. M. Herrmann and J. C. Vedrine: Appl. Catal. **16** (1985) 315.
7) D. R. Pyke, R. Reid and R. J. D. Tilley: J. Chem. Soc. Farad. Trans. I **76** (1980) 1174.
8) T. Nütz and M. Haase: J. Phys. Chem. B **104** (2000) 8430.
9) G. Boschloo and D. Fitzmaurice: J. Phys. Chem. B **103** (1999) 3093.
10) S. Akselrod, M. Pasternak and S. Bukshpan: Phys. Rev. B **11** (1975) 1040.
11) J. Rockenberger, U. zum Felde, M. Tischer, L. Tröger, M. Haase and H. Weller: J. Chem. Phys. **112** (2000) 4296.
12) S. Tiwari, F. Rana, H. Hanafi, A. Hartstein, E. F. Crabbe´, K. Chan: Appl. Phys. Lett. **68** (1996) 1377.
13) K. Yano, T. Ishii, T. Hashimoto, T. Kobayashi, F. Murai and K. Seki: IEDM Tech. Dig. (1993), p. 541.
14) C. Gabrielli: Technical Report No. 004/83, (Solartron Instruments, England, 1998).

15) For general reference see, *Impedance Spectroscopy; Theory, Experiment, and Applications,* ed. E. Barsoukov and J.R. Macdonald (Wiley Interscience Publications, 2005) 2nd ed., Sect. 2.1.6.1, p. 76.

16) T. Oi, M. Endoh, M. Narimoto and M. Hosoe: J. Mater. Sci. **35** (2000) 509.

17) M. Bagheri-Mohagheghi and M. Shokooh-Saremi: Semicond. Sci. Technol. **19** (2004) 764.

18) L. Jingyue and J. P. Coleman: Mater. Sci. Eng. A **286** (2000) 144.

**Table I.** Electrochemical impedance analysis. For data collection 5 mV rms voltage was used. Sample 1 and Sample 2 contained different particle size distributions (see Table II).

| Sample description | $R_S$ (Ω) | C (μF) | $R_P$ (Ω) | W ($\Omega/sec^{0.5}$) | $X^2$ |
|---|---|---|---|---|---|
| | | *Sample 1* | | | |
| Fresh | 13.5(1) | 9(6) | 0.5(1) | 65(1) | $8.7x10^{-5}$ |
| Yellowed | 16.4(2) | 7(2) | 1.9(2) | 200(4) | $2.8x10^{-4}$ |
| Yellowed (2 yr.) | 300(100) | 0.00005(2) | 700(100) | 20000(2400) | $1.3x10^{-2}$ |
| | | *Sample 2* | | | |
| Fresh | 24(1) | 0.3(2) | 8(1) | 100(20) | $4.9x10^{-3}$ |
| Yellowed | 27(2) | 0.13(6) | 12(2) | 400(50) | $6.6x10^{-3}$ |

**Table II.** Summary of experimental results for Powder X-Ray Diffraction ($SnO_2$) and Atomic Absorption measurements for Samples 1 and 2. Common antimony oxides, i.e., $Sb_2O_3$ (Senamontite), $SB_2O_4$ (α-Cervantite, β-Clinocervantite, β-Cervantite), and $Sb_2O_5$, exhibit reflections at $27.7^o$, ($25.8^o$, $27.7^o$, $27.5^o$) and $27.3^o$, respectively; hence the additional peak (at $26.6^o$) may originate from a distorted Casserite structure.[a]

| | Condition | Peak position (3σ) | | Crystal size[e] (nm) | | Etched material (μg/cm$^2$ Cathode) | |
|---|---|---|---|---|---|---|---|
| | | **1** | **2** | **1** | **2** | **Sn** | **Sb** |
| Sample 1 | Untreated | 26.52(1) | 26.66(1) | 41(4) | 8.7(3) | 12 [4] | 50 [8] |
| | Chem. Oxidized[b] | 26.54(1) | 26.69(1) | 38(3) | 8.4(3) | | |
| | Oxidized[c] (e) | 26.56(1) | 26.59(1) | 24(1) | 4.58(5) | | |
| | Reduced[d] (e) | 26.55(1) | 26.53(1) | 27(2) | 4.5(3) | | |
| Sample 2 | Untreated | 26.57(1) | 26.66(1) | 32(5) | 3.9(1) | 0.8 [0.7] | 36 [7] |
| | Chem. Oxidized | 26.55(1) | 26.59(1) | 30(4) | 4.0(1) | | |
| | Oxidized (e) | 26.62(2) | 26.63(1) | 19(3) | 3.9(1) | | |
| | Reduced (e) | 26.55(1) | 26.62(1) | 28(4) | 4.1(1) | | |

[a] Numbers in parenthesis give standard deviations for the last quoted digit.
[b] Chemical oxidation was accomplished by coating the devices with ordinary household bleach.
[c,d] Electrochemical (e) oxidation and reduction was carried out by charging the devices in a LiCl bath for a period of 72 h at 1.5 V.
[e] The crystal size (t) was evaluated using the Debye-Scherrer equation.

Figure captions

**Figure 1.** Schematic Diagram illustrating the 'side-by-side' design of a printed electrochromic display[18]. (Color Printing)

**Figure 2**. (a) Sn Mössbauer spectra from control (bottom) sample 1 and aged (top) sample 3 electrodes: The peaks are only observed at 0.00 mm/s corresponding to Sn(IV). [Tin isomer shift (IS) values (peak position) of about 2.6 mm/s, 2.6-4.6 mm/s and –0.3-1.9 mm/s for Sn(0), Sn(II) and Sn(IV), respectively]. (b) First derivative Sb XANE spectra from fresh and aged devices, along with spectra from model compounds, $Sb_2O_3$ and $Sb_2O_4$ (a mixture of $Sb_2O_3$ and $Sb_2O_5$). The fresh and aged samples only shows the presence of Sb(V).

**Figure 3.** (a) Plots of contrast ratios vs Voltage depicting hysteresis. The "coercive" voltage $V_c$ is approximately 0.2 V (see text). (b) Development of b* during charging, where the slope of b* vs ln(t) is 0.53±0.04 for both curves.

**Figure 4.** Impedance spectra from ATO EC fresh (left) and yellowed (right) cells. Lines indicate best fit obtained from Zsimp. [The data was fitted to the Randle's equivalent circuit model (inset) from Zsimp].

**Figure 5.** NLSFIT of three Gaussians for reflections in the 24-29° (2θ) region from the EC devices. Vertical lines indicate peak positions. The dotted and dashed lines show the deconvoluted peaks arising from large size (dotted) and smaller size (dashed) nanoparticles. The thick shaded curve corresponds to $TiO_2$ reflection, which provided an internal calibration standard for 2θ scale.

Color Printing

**Figure 1.**

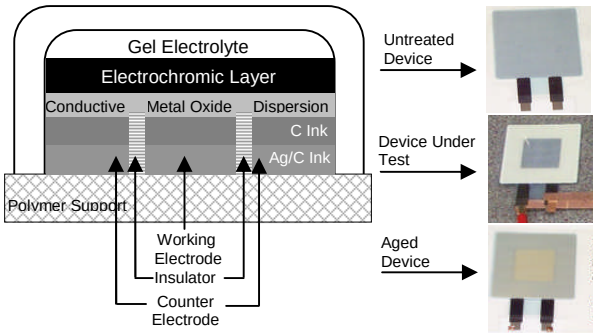

**Figure 2**.

(a)

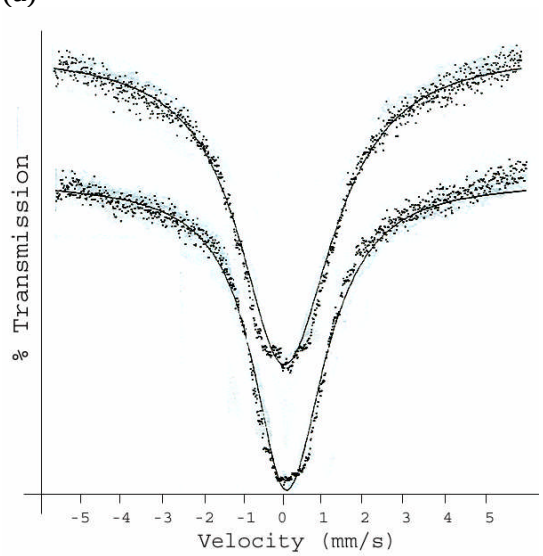
% Transmission
-5 -4 -3 -2 -1 0 1 2 3 4 5
Velocity (mm/s)

(b)

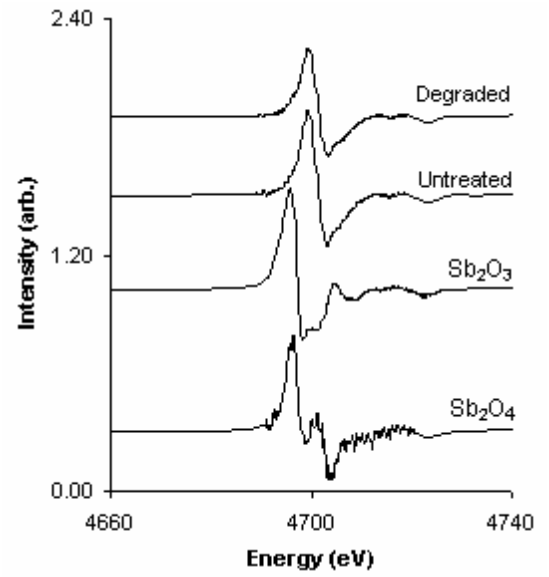
2.40
1.20
0.00
Intensity (arb.)
Degraded
Untreated
Sb2O3
Sb2O4
4660
4700
4740
Energy (eV)

**Figure 3.**

(a)

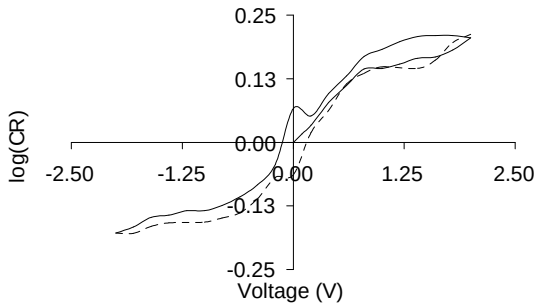
0.25
0.13
0.00
-0.13
-0.25
-2.50
-1.25
0.00
1.25
2.50
log(CR)
Voltage (V)

(b)

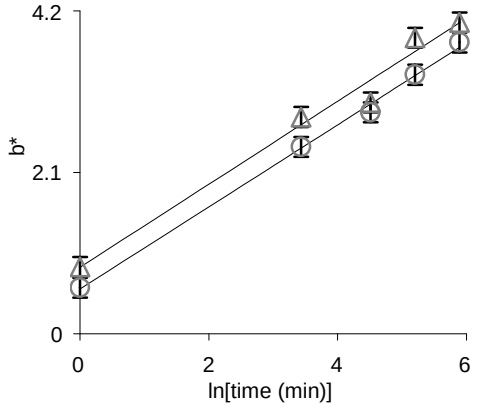
4.2
2.1
0
b*
0
2
4
6
ln[time (min)]

**Figure 4.**

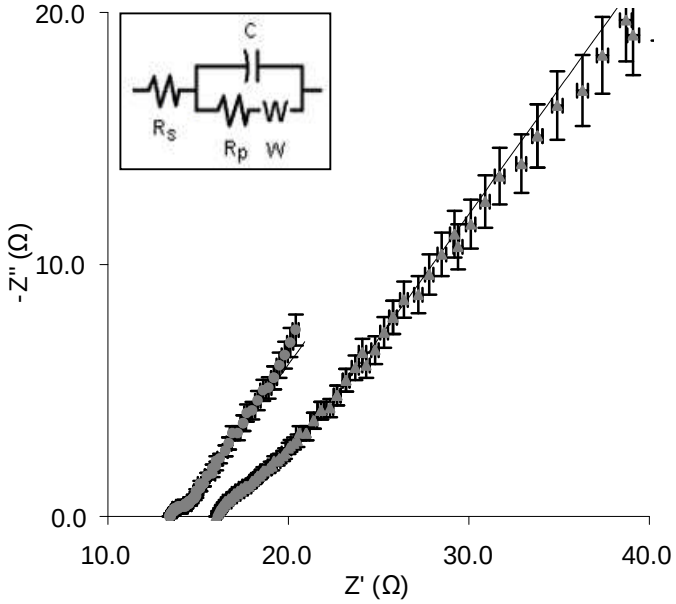

**Figure 5.**

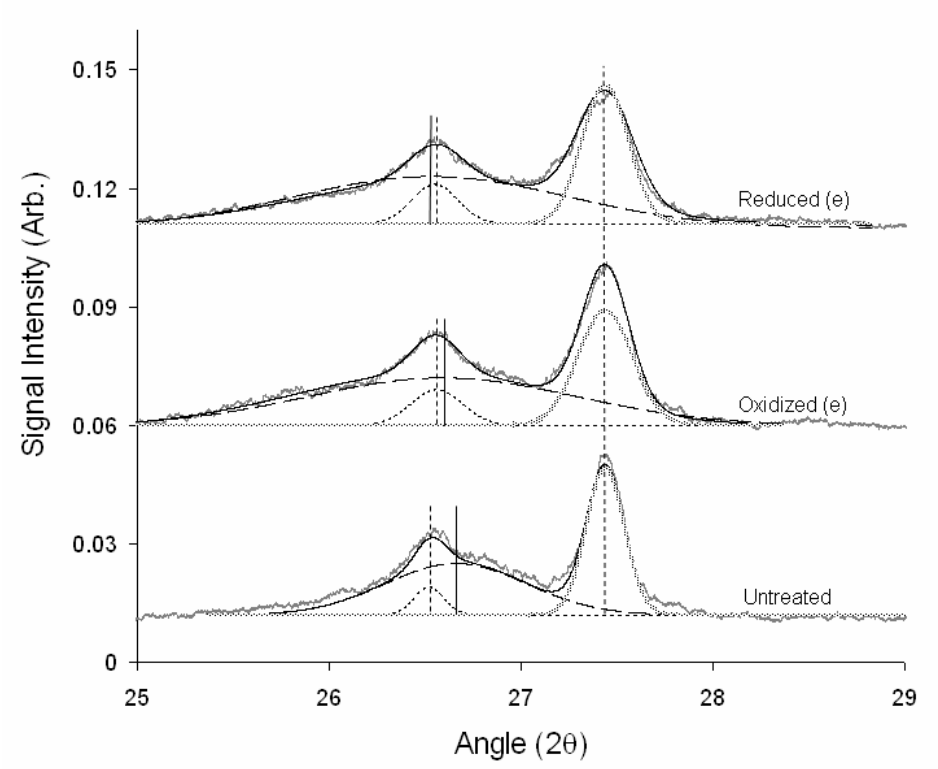
0.15
0.12
0.09
0.06
0.03
0
Signal Intensity (Arb.)
Reduced (e)
Oxidized (e)
Untreated
25
26
27
28
29
Angle (2θ)